Domain growth kinetics in the isosceles triangular Ising antiferromagnet $CoNb_2O_6$

S. Kobayashi,* H. Okano, T. Jogetsu, J. Miyamoto, and S. Mitsuda
Department of Physics, Tokyo University of Science, Kagurazaka, Shinjuku-ku, Tokyo 162-8601, Japan
(Received 24 September 2003; published 30 April 2004)

We have studied the domain-growth kinetics of fourfold-degenerate antiferromagnetic (AF) and threefold-degenerate ferrimagnetic states in the isosceles triangular Ising antiferromagnet $CoNb_2O_6$ by ac susceptibility measurements and Monte Carlo simulations. In both magnetic phases ac susceptibility after the field quench is found to decrease with time according to the power-growth law with an universal growth exponent $n=0.21 \pm 0.01$. The prefactor in the power-growth law suggests that the zero-field growth of the AF state is strongly suppressed by the application of magnetic fields along the direction perpendicular to the frustrated isosceles-triangular lattice. Monte Carlo results show the unusual domain growth dominated by the reversal of the *free* magnetic spins near favorable domain walls where the exchange field is effectively canceled out due to the isosceles triangular geometry of spins. The obtained domain configuration strongly supports our neutron-diffraction results that revealed the temporal shift of the magnetic Bragg peak position during the growth.

DOI: 10.1103/PhysRevB.69.144430 PACS number(s): 75.25.+z, 05.70.Ln, 75.40.Mg

I. INTRODUCTION

The kinetics of domain growth toward the equilibrium state for nonconserved order parameter has been widely studied.[1,2] For the Ising system with twofold-degenerate ground states (degeneracy $p=2$), it is well established that the domain growth proceeds with time as $t^{1/2}$ owing to the curvature-driven force. This power-law time dependence is universal, being independent of the microscopic interactions and the lattice geometry.[3]

In the Ising system with highly degenerate ground states, the situation is not simple.[3] Since the system can order in several thermodynamically equivalent ordered states, the domain growth proceeds through the competition between the different ordered domains which were nucleated simultaneously just after the quench. From Monte Carlo (MC) simulations for the two-dimensional (2D) anisotropic next-nearest-neighbor Ising (ANNNI) model for $(p\times 1)$ uniaxial phases with $p=3$[4] and $p=4$,[5–7] it appeared that several types of domain walls in the modulated direction influence the domain-growth kinetics. During the domain growth, energetically favorable domain walls persist, which make the growth kinetics slower and, in some cases, spatially anisotropic.

Despite these numerical works, only a few experimental work on the domain growth kinetics of the large degenerate ground states are reported to date. In this paper, we present the detailed study of the domain growth kinetics of highly degenerate ground states in $CoNb_2O_6$ by ac susceptibility measurements and Monte Carlo simulations. As shown in Fig. 1, in $CoNb_2O_6$ 1D ferromagnetic zigzag chains running along the c axis arrange in an isosceles triangular geometry in the a-b plane. At low temperatures, Co spins are confined to two different easy axes in the nearly a-c plane with a canting angle of θ_0 $(=31°)$ from the c axis, and various magnetically ordered phases characterized by a propagation wave vector $q_{\mathrm{propa}}=(0\ q\ 0)$ appear; fourfold-degenerate antiferromagnetic (AF) phase $(q=\frac{1}{2})$, field-induced threefold-degenerate ferrimagnetic (FR) phase $(q=\frac{1}{3})$, and sinusoidally amplitude-modulated incommensurate (IC) phase $(\frac{1}{3}<q<\frac{1}{2})$. As our previous works[8] demonstrated, this system is characterized by an isosceles triangular lattice Ising model with an Ising Hamiltonian given by

$$\mathcal{H}=-J_0\sum_{i,j}\mathbf{S}_i\cdot\mathbf{S}_j-J_1\sum_{i,j}\mathbf{S}_i\cdot\mathbf{S}_j-J_2\sum_{i,j}\mathbf{S}_i\cdot\mathbf{S}_j$$
$$-J_3\sum_{i,j}\mathbf{S}_i\cdot\mathbf{S}_j-g\mu_{\mathrm{B}}\sum_{j}\mathbf{S}_j\cdot\mathbf{H}_{\mathrm{ex}}, \qquad (1)$$

where $\mathbf{H}_{\mathrm{ex}}$ is an external magnetic field and $g=2.1$. $\mathbf{S}_i$ is the spin with $S=\frac{3}{2}$ and the summation is taken over the pairs of spins. The ferromagnetic intrachain exchange interaction along the c axis, and nearest- and next-nearest-neighbor antiferromagnetic interchain exchange interactions are given by $J_0/k_{\mathrm{B}}=0.6015$ K, $J_1/k_{\mathrm{B}}=-0.0508$ K, and $J_2/k_{\mathrm{B}}=-0.0812$ K, respectively. Further neighbor ferromagnetic interchain interaction J_3 (>0) which is considered to be weak compared with J_1 and J_2, is necessary for stabilizing magnetic correlations along the a axis in the AF phase below $T_2\sim 1.9$ K [Fig. 1(a)]. Since a ratio of effective antiferro-

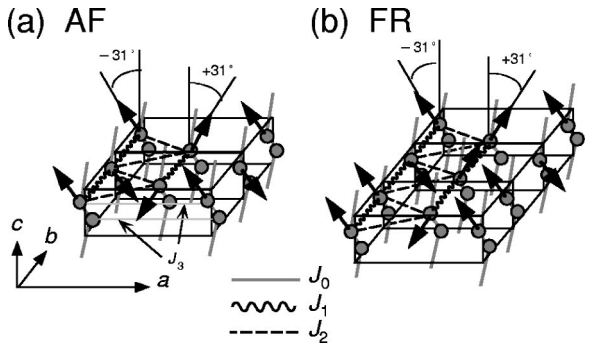

FIG. 1. Magnetic structure in (a) fourfold-degenerate AF and (b) threefold-degenerate FR phases. The solid arrows show Co spins, confined to the two different easy axes. The zigzag chains running along the c axis form an isosceles triangular lattice with interchain antiferromagnetic interactions J_1 and J_2 in the a-b plane.

magnetic interactions $J_2\cos 2\theta_0/J_1$ is 0.75 and close to 1.0 of a triangular Ising antiferromagnet, the system can be regarded as an Ising antiferromagnet with a partially released triangular geometrical frustration.

Recently, we performed neutron scattering and ac susceptibility measurements at $T=1.5$ K under low applied fields along the c axis.[9] Neutron scattering directly showed that in the AF phase the domain growth after the field quench proceeds according to the power law with anomalously low growth exponent $n\sim 0.2$. We found that the domain growth along the b axis proceeds faster than along the a axis and is strongly suppressed by the application of magnetic fields.[10] Simple arguments about an activation energy showed that the domain-wall motion, mediated by the reversal of energetically free magnetic chains close to the domain wall in the b direction, results in the spatially anisotropic domain growth. Moreover, the time dependence of the ac susceptibility data revealed the power-law growth with $n=0.21\pm 0.01$ in the AF phase and also at the specific field H_s ($=1214$ Oe) in the FR phase where the extra anomaly of the susceptibility was detected in the field-increasing scan after zero-field cooling (ZFC).

In this paper, we examine the domain-growth kinetics of the fourfold-degenerate AF and threefold-degenerate FR states by ac susceptibility measurements under magnetic fields up to 2 kOe along the c axis. The measurements of ac susceptibility not only give useful information about the time dependence of the number of free magnetic chains which plays a crucial role for the domain growth in this system, but also allow us to precisely determine the growth law owing to the time-resolved measurements. We will show that the time dependence of the in-phase susceptibility follows the power law with universal growth exponent $n=0.21\pm 0.01$ in both magnetically ordered phases. The analysis of the relaxation data, combined with field-jump measurements show that the application of the magnetic field strongly suppresses the domain growth along the b axis in the AF phase, while this is not effective around H_s in the FR phase. Monte Carlo simulations for an isosceles triangular lattice Ising model show that this originates from the different growth mechanism in the FR phase; two types of energetically favorable domain walls compete throughout the domain growth in the FR phase while only single type of domain wall dominates in the AF phase. The time dependence of the AF Bragg peak position observed in our neutron-diffraction study is well explained by our Monte Carlo results where the domain configuration along the b axis with a $\pi/2$ phase shift was obtained.

The organization of the paper is as follows. In Sec. II, we present the possible types of domain walls between thermodynamically equivalent domain walls in both AF and FR phases and give simple energy considerations. In Sec. III A we present experimental details of ac susceptibility measurements. Then the ac susceptibility data in the AF and FR phases are discussed in Secs. III B and III C, respectively. Section IV describes MC simulation results. Section IV A treats MC simulation procedure and gives magnetic phase diagram determined. Sections IV B and IV C devote to the MC results of the domain-growth kinetics in the AF and FR phases, respectively. Finally, we present our conclusion in Sec. V.

II. ENERGY CONSIDERATIONS OF DOMAIN WALLS

A. Fourfold-degenerate AF phase

As seen in the AF structure shown in Fig. 1(a), ferromagnetic 1D chains along the c axis align antiferromagnetically along the b axis and form magnetic unit cell doubling of chemical unit cell along the b axis. Since in the magnetic unit cell there exist nonequivalent four 1D chains, the ground state of the AF state is fourfold degenerated. Consequently, just after the quench, thermodynamically equivalent four AF domains nucleate and various types of domain walls will be formed. In this section, we present possible types of domain walls during the domain growth in the AF phase and discuss the activation energy of magnetic chains close to the domain walls, which is used to interpret ac susceptibility data and Monte Carlo results shown later.

Figures 2(a)–2(e) show possible types of domain walls in the b and a directions in the AF phase. To distinguish four AF domains, we symbolically labeled those domains as A, B, C, and D; the projection of Co spin on the b-c plane is described by a sine-wave form of $\sim\sin[\pi(y+\frac{1}{4})+\phi]$ with a phase $\phi=0$, $-\pi/2$, π, $+\pi/2$, respectively, as shown in Fig. 2(f), where y is a coordinate of spin in the b direction. In Figs. 2(a)–2(e), the site dependence of the activation energy of magnetic chain in zero field is also given. The activation energy, which was calculated within J_1 and J_2, was defined as an energy per Co spin to be required in order to reverse a magnetic chain at each site. The magnetic chain with a positive (zero) activation energy is energetically stable (free) and requires a finite (no) activation energy to reverse while that with a negative activation energy is energetically unstable and is expected to reverse immediately after the domain wall is formed. The site dependence of the activation energy of the domain wall between A and B domains, A/B shown in Fig. 2(a), is possible also for the B/C, C/D, D/A domain walls. Therefore, we call these domain walls A/B type. Similarly, energetically nonequivalent A/C-, A/D-, and B/D-type domain walls exist in the b direction. As is seen for the case of the A/D-type in Fig. 2(f), the domain wall belonging to same type satisfies same phase-shift condition at the boundary; the A/B-, A/C-, A/D-, and B/D-type domain walls result in the phase shift of sine-wave modulation by $\pi/2$, π, $\frac{3}{2}\pi$, and π, respectively. On the other hand, in the a direction, all the domain walls are energetically equivalent within J_1 and J_2.

Just after the quench, energetically unfavorable domain walls will rapidly diminish and energetically favorable one will persist throughout the domain growth. As shown in Fig. 2, both A/B-type and A/C-type domain walls in the b direction include energetically unstable magnetic chains close to the domain wall. Therefore, at the early stage, those unstable chains will reverse rapidly, and the A/B- and A/C-type domain walls decay to a combination of the A/D-type domain wall, $A/D/C/B$ and $A/D/C$, respectively. The transition from unstable domain wall to stable one is known as wetting

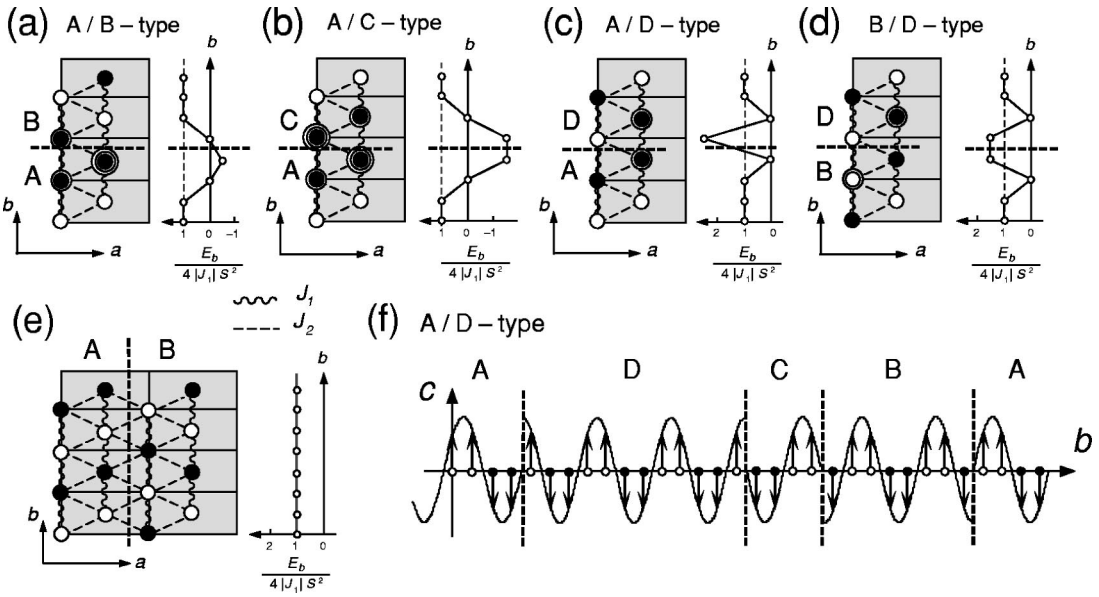

FIG. 2. Energetically different types of domain walls in (a)–(d) *b* and (e) *a* directions at zero applied field in the AF phase. The A/B-type includes the A/B, B/C, C/D, D/A domain walls, and the A/C-type includes the A/C, C/A domain walls, and the A/D-type includes the A/D, D/C, C/B, B/A domain walls, and the B/D-type includes the B/D, D/B domain walls. The open and closed circles denote up and down magnetic chains, and the thick dashed lines represent domain wall. The magnetic chains depicted by double circles show energetically free magnetic chains in zero field while those depicted by triple circles show unstable magnetic chains. An activation energy of a magnetic chain at each site to be reversed in zero field, which was calculated within J_1 and J_2, is also given. (f) An example of a domain-wall configuration due to the A/D type in the *b* direction. The solid arrows show the projection of Co spin on the *b*-*c* plane. At each domain-wall position, the phase of the sine-wave modulation is shifted by $+\pi/2$.

transition and was commonly observed for the ANNNI model.[5] On the other hand, in the case of the A/D- and B/D-type domain walls in the *b* direction, the reversal of energetically free magnetic chains, on which the exchange field by J_1 and J_2 is canceled out, plays a crucial role. Particularly, for the B/D-type domain wall, certain reversal process of free magnetic chains eventually results in the combination of the A/D-type domain wall. Therefore, in the AF phase, the A/D-type domain wall in the *b* direction is expected to dominate the domain growth along the *b* axis.

B. Threefold-degenerate FR phase

As shown in Fig. 3, recently, the extra anomaly of the ac susceptibility was observed at the specific field $H_s \sim 1214$ Oe in the FR phase in the field-increasing scan after ZFC. Interestingly, as shown in the inset in Fig. 3, this anomaly showed up only in the field-increasing scan at low temperatures after ZFC, while it was not detected both in the field-decreasing scan at $T=1.5$ K after field cooling (FC) at $H=2$ kOe and in the high-temperature field-increasing scan at $T=1.9$ K after ZFC. Within the mean-field theory this specific field H_s is very close to the exchange field $2J_1/g\mu_B\cos\theta_0$ ($=1260$ Oe). Therefore, H_s can be regarded as the magnetic field where the exchange field from two antiferromagnetically coupled spins through J_1 becomes of the same magnitude as the applied field. However, this anomaly cannot be explained when the formation of the FR long-range order is assumed. Therefore, this anomaly of the in-phase susceptibility is considered to originate from the thermal fluctuation of magnetic chains near the domain walls which become free to reverse at H_s. Note that similar small peak of the susceptibility in the threefold-degenerate FR phase has been reported for $CoCl_2 \cdot H_2O$ (Ref. 11) and $CoBr_2 \cdot H_2O$,[12] where the twofold-degenerate antiferromagnetic state is stabilized as the zero-field ground state.

Figures 4(a)–4(d) show possible types of domain walls and the site dependence of the activation energy of a magnetic chain at H_s in the FR phase. As can be seen in Fig. 4(e), thermodynamically equivalent three FR domains with the phase $\phi=0,+\frac{2}{3}\pi,-\frac{2}{3}\pi$ in a sine-wave form of $\sim\sin[\frac{4}{3}\pi(y+\frac{1}{8})+\phi]$ are symbolically labeled as A', B', C', respectively. As shown in Fig. 4, the C'/A'-type domain

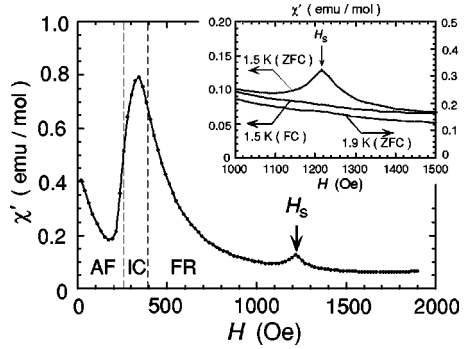

FIG. 3. In-phase susceptibility χ' as a function of the magnetic field at $T=1.5$ K after ZFC. The inset shows the enlargement around H_s where χ' at $T=1.5$ K both after FC at $H=2$ kOe and ZFC, and at $T=1.9$ K after ZFC, are shown.

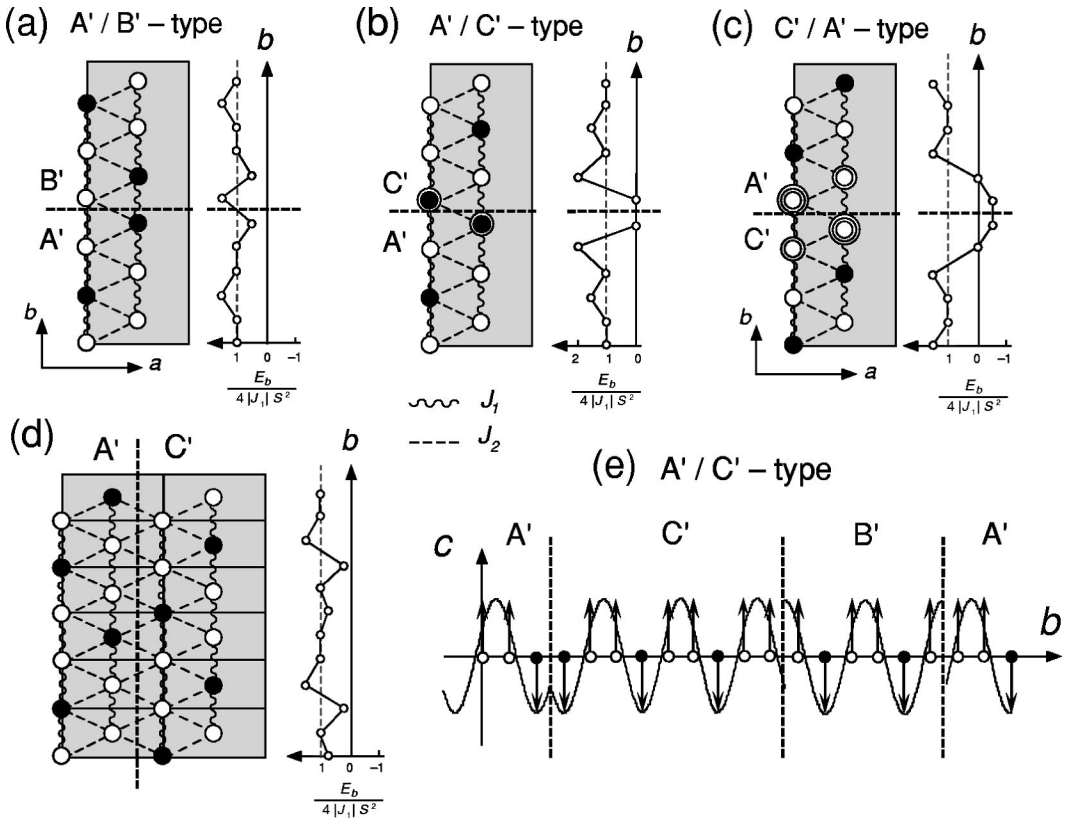

FIG. 4. Energetically different types of domain walls in (a)–(c) *b* and (d) *a* directions at H_s in the FR phase. Within J_1 and J_2 all the domain walls in the *a* direction are energetically equivalent. An activation energy of a magnetic chain to be required to reverse at $H=H_s$, calculated within J_1 and J_2, is also shown. The A'/B' type includes the A'/B', B'/C' domain walls, and the A'/C' type includes the A'/C', C'/B', B'/A' domain walls, and the C'/A' type includes the C'/A' domain wall. Although both the C'/B' and B'/A' domain walls give different site dependence of the activation energy of a magnetic chain from that of the A'/C' one, those walls were included in the A'/C' type, because all the C'/B', B'/A', and A'/C' domain walls are energetically equivalent. The open and solid circles represent up and down magnetic chains, respectively. The magnetic chains depicted by double circles show energetically free magnetic chains at H_s while those depicted by triple circles show unstable magnetic chains around H_s. (e) An example of a domain-wall configuration due to the A'/C'-type in the *b* direction. The solid arrows show the projection of Co spin on the *b*-*c* plane. At each domain-wall position, the phase of the sine-wave modulation is shifted by $-\frac{2}{3}\pi$.

wall which includes two unstable up magnetic chains is energetically unstable at H_s. Therefore, the C'/A'-type domain wall will decay to the A'/B'-type domain wall through the reversal of unstable magnetic chains, and two types of domain walls (A'/B' and A'/C' types) is expected to play an important role around H_s. Since at H_s the magnetic chain close to the A'/C'-type domain wall can reverse freely, the extra anomaly of the susceptibility at H_s is considered to originate from the thermal fluctuation of free magnetic chains near the A'/C'-type domain wall which were produced after passing through the first-order IC-FR phase transition in the increasing magnetic field. The presence of the domain walls even at H_s might reflect the fact that the formation of infinitely long-range up-up-down FR networks from the IC sinusoidal structure requires the complicated rearrangement of up and down magnetic chains, and is difficult at low temperatures in particular where the thermal fluctuation of spins becomes less effective. Since among the favorable A'/B'- and A'/C'-type domain walls only the A'/C'-type domain wall includes free magnetic chains around H_s, the measurements of the ac susceptibility after the quench will give information mainly about the A'/C'-type one.

III. AC SUSCEPTIBILITY RESULTS

A. Experiment

Ac susceptibility measurements were performed under magnetic fields along the *c* axis up to 2 kOe down to $T=1.5$ K. Since the ac susceptibility is sensitive to the thermal fluctuation of spins, it is considered that the observed susceptibility is proportional to the number of free magnetic chains during the domain growth which are formed around the domain wall in the *b* direction.

The single crystal of $CoNb_2O_6$ was prepared with flux-growth technique and has dimensions $2.5\times2.5\times7.5$ mm^3. An ac field of 0.69 Oe parallel to the magnetic field was applied at the frequency 523 Hz. We checked that the domain-growth law deduced from ac susceptibility data is independent of frequency and is not influenced by ac field.

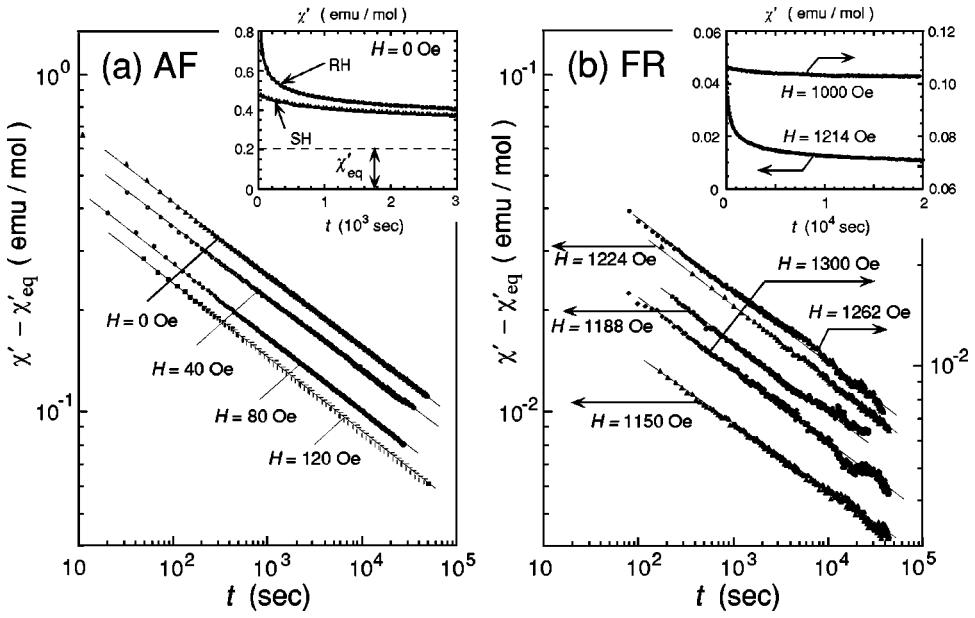

FIG. 5. Double-logarithmic plots of $\chi'(t)-\chi'_{eq}$ (a) around zero field in the AF phase and (b) around $H_s=1214$ Oe in the FR phase. Inset in (a) shows $\chi'(t)$ in zero field after RH and SH. The equilibrium in-phase susceptibility χ'_{eq} was obtained by fitting the data to Eq. (2). Inset in (b) shows $\chi'(t)$ at H_s and $H=1000$ Oe.

To obtain a nonequilibrium state, the magnetic field was rapidly removed from the field-induced FR state at $H=600$ Oe with a sweep rate of 100 Oe/sec, at each measuring temperature. Just after reaching the zero field, the magnetic field was applied up to each measuring field in the AF case while in the FR case the sample was subjected to stay at $H=1224$ Oe ($\sim H_s$) before the measurements at the desired field start. This treatment which we refer to as RH has the same effects as the rapid-cooling treatment from paramagnetic (PM) state above T_1 and has good reproducibility of measuring data. We defined the origin of time as the time where the magnetic field was reached at the measuring field and monitored time dependence of the ac susceptibility in the time range up to 8×10^4 sec.

B. Fourfold-degenerate AF phase

In the inset in Fig. 5(a), we show the time dependence of the in-phase susceptibility $\chi'(t)$ in zero field, taken after RH and slowly decreasing field (SH) from $H=600$ Oe with a sweep rate of 0.13 Oe/sec. On the time scale of the order of an hour, $\chi'(t)$ decreases with time and gradually approaches the equilibrium susceptibility χ'_{eq}. At $t\sim 0$, $\chi'(t)$ for RH largely exceeds that for SH, indicating that a large number of domain walls in the b direction remains just after RH. This result agrees with the neutron-scattering results[9] that the RH procedure yields small domain size along the b axis at $t\sim0$ compared with that of equilibrium state.

Figure 5(a) shows the log-log plot of $\chi'(t)$ at $T=1.5$ K under low applied fields in the AF phase. For all measuring fields, $\chi'(t)$ shows an expected linear behavior, indicating the power-law time dependence of $\chi'(t)$. Assuming that the time-dependent part of in-phase susceptibility results from the thermal fluctuation of free magnetic chains, the power-law equation for $\chi'(t)$ is given by

$$\chi'(t,H)=\chi'_{eq}(H)+\chi'_{free}(H)[\alpha(H)t^{-n}], \qquad (2)$$

where χ'_{free} is an in-phase susceptibility of a free magnetic chain, being temperature- and magnetic-field dependent. The prefactor $\alpha(H)$ means the number of free magnetic chains at $t=1$ and is the measure of relaxation speed. Irrespective of the strength of the magnetic field, an almost equal growth exponent $n=0.21\pm0.01$ was obtained as shown in Fig. 6(a), which is in good agreement with $n\sim0.2$ of our neutron-scattering results.[9] As previous neutron-scattering studies[9] revealed, the domain growth along the b axis is suppressed in the AF phase by the application of magnetic field. This implies that the prefactor $\alpha(H)$ which is proportional to the number of free magnetic chains increases with increasing the magnetic field. However, the power-law fits of the relaxation

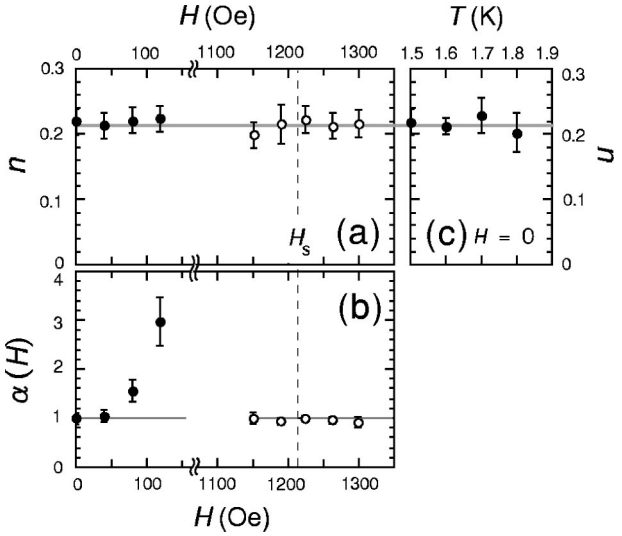

FIG. 6. Magnetic-field dependence of (a) growth exponent n and (b) prefactors $\alpha(H)/\alpha(H=0$ Oe) and $\alpha(H)/\alpha(H=1224$ Oe) of the AF and FR states, obtained from the ac susceptibility measurements. The solid and open circles show the data of the AF and FR states, respectively. (c) Temperature dependence of growth exponent n in zero field.

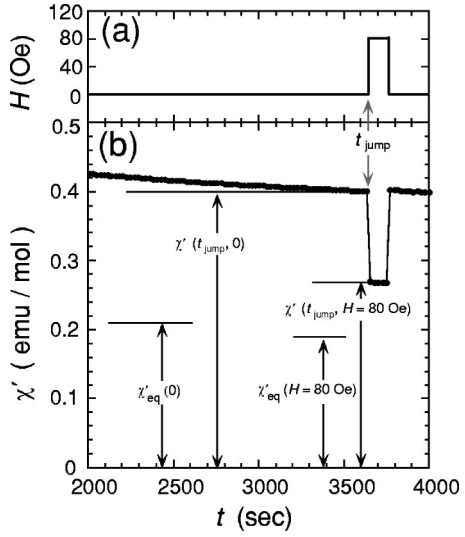

FIG. 7. An example of the field-jump susceptibility measurement after RH. (a) Time dependence of applied fields. The magnetic field rapidly changes from 0 Oe to 80 Oe at $t_{\mathrm{jump}}=3650$ sec, and returns to zero field after 100 sec. (b) Time dependence of the in-phase susceptibility observed in this field-jump measurement.

data shown in Fig. 5 only give the absolute value of $[\chi'_{\mathrm{free}}\,\alpha(H)]$ and the magnetic-field dependence of $\alpha(H)$ cannot be determined. Therefore, to extract $\alpha(H)$ from the observed data, it is indispensable to determine χ'_{free} at all measuring fields.

To estimate χ'_{free}, we performed the field-jump measurements at $T=1.5$ K, where at time $t_{\mathrm{jump}}=3650$ sec during the relaxation process in zero field the magnetic field was jumped to the desired field and then the susceptibility at this field was measured promptly. As an example, the field-jump data for the $H=80$ Oe case is shown in Fig. 7. When the magnetic field is changed to $H=80$ Oe from zero field at t_{jump}, the in-phase susceptibility abruptly decreases. Since the number of free magnetic chains at t_{jump}, being proportional to $[\chi'(t_{\mathrm{jump}},0)-\chi'_{\mathrm{eq}}(0)]/\chi'_{\mathrm{free}}(0)$, is conserved at t_{jump}, the following equation can be obtained:

$$\frac{\chi'(t_{\mathrm{jump}},0)-\chi'_{\mathrm{eq}}(0)}{\chi'_{\mathrm{free}}(0)}=\frac{\chi'(t_{\mathrm{jump}},H)-\chi'_{\mathrm{eq}}(H)}{\chi'_{\mathrm{free}}(H)}, \qquad (3)$$

where $\chi'_{\mathrm{eq}}(H)$ is the value determined from the power-law fittings of the relaxation data. From this equation, the ratio of in-phase susceptibility of free magnetic chain, $\chi'_{\mathrm{free}}(H)/\chi'_{\mathrm{free}}(0)$, was determined experimentally. Note that in present study absolute value of $\chi'_{\mathrm{free}}(H)$ was not determined, because the exact number of free magnetic chains during the domain growth is not clear. With increasing the magnetic field, $\chi'_{\mathrm{free}}(H)/\chi'_{\mathrm{free}}(0)$ was found to decrease monotonically, being qualitatively consistent with the behavior of the 1D magnetic chain with nearest-neighbor ferromagnetic intrachain interaction.

Dividing Eq. (2) for H by that for zero field, and using Eq. (3), the prefactor at H is given, using $\alpha(0)$, by

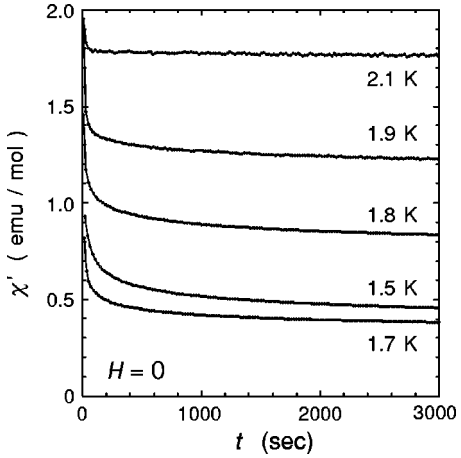

FIG. 8. $\chi'(t)$ at zero field after RH, taken at temperatures below and just above $T_2=1.9$ K. For clarity, the data at $T=1.9$ K and 2.1 K are shifted by -1.0 and -3.5, respectively.

$$\frac{\alpha(H)}{\alpha(0)}=\frac{[\chi'_{\mathrm{free}}(H)\alpha(H)]_{\mathrm{fit}}}{[\chi'_{\mathrm{free}}(0)\alpha(0)]_{\mathrm{fit}}}\,\frac{\chi'(t_{\mathrm{jump}},0)-\chi'_{\mathrm{eq}}(0)}{\chi'(t_{\mathrm{jump}},H)-\chi'_{\mathrm{eq}}(H)}. \qquad (4)$$

Here $[\cdots]_{\mathrm{fit}}$ is the value obtained by fitting the relaxation data of Fig. 5(a) to Eq. (2).

By performing the field-jump measurements at all measuring fields, the magnetic-field dependence of $\alpha(H)/\alpha(0)$ was determined as shown in Fig. 6(b). With increasing magnetic field from zero field, $\alpha(H)/\alpha(0)$ increases dramatically. This suggests that large number of free magnetic chains, i.e., A/D-type domain wall remain during the domain growth by the application of magnetic fields. This slow growth under the magnetic field is interpreted as due to the fact that the A/D-type domain walls become less mobile owing to the finite activation energy of free magnetic chains to reverse against the magnetic field. The observed data are qualitatively consistent with the magnetic-field dependence of the prefactor of the power-growth law determined from magnetic correlation length along the b axis.[9]

With increasing temperature from $T=1.5$ K in zero field, on the other hand, the decrement of $\chi'(t)$ with time drastically reduces and the relaxation is restricted within the very narrow time interval of several minutes just after RH as shown in Fig. 8. At $T=2.1$ K above T_2, $\chi'(t)$ is almost equilibrium value just after the quench and no significant temporal behavior of $\chi'(t)$ was detected. This results indicate the fast relaxation process at higher temperatures. $\chi'(t)$ well fitted to the power law of Eq. (2) and the same growth exponent to that at $T=1.5$ K was obtained irrespective of the temperature as shown in Fig. 6(c). This suggests that the power-growth law with $n=0.21$ is maintained all over the AF phase.

C. Threefold-degenerate FR phase

In the inset in Fig. 5(b), we show the time dependence of $\chi'(t)$ at $T=1.5$ K both at H_s and $H=1000$ Oe far from H_s obtained after RH. While $\chi'(t)$ at $H=1000$ Oe is weakly

time dependent, that at H_s dramatically decreases with time. This means that the domain-growth kinetics at H_s is dominated by the magnetic chains which can reverse freely at H_s as discussed in Sec. II B.

Figure 5(b) shows the log-log plot of $\chi'(t)$ around H_s in the FR phase. $\chi'(t)$ decreases with the power-law time dependence at all measuring fields. As shown in Fig. 6(a), the power-law fits gave the growth exponent $n=0.21\pm0.01$, being equal to that of the AF state with fourfold-degenerate ground states.

Moreover, to investigate the behavior of $\alpha(H)$ around H_s, field-jump measurements were also performed. In this case, the magnetic field was jumped at $t_{\rm jump}$ from $H=1224$ Oe close to H_s toward a desired field, and the magnetic-field dependence of $\alpha(H)/\alpha(H=1224\ {\rm Oe})$ was determined. In contrast to the dramatic increase of $\alpha(H)$ with increasing magnetic field in the AF phase, $\alpha(H)/\alpha(H=1224\ {\rm Oe})$ is nearly field independent around H_s as shown in Fig. 6(b). Taking account that around H_s $\chi'(t)$ reflects the number of free magnetic chains around the A'/C'-type domain wall, the annihilation speed of the A'/C'-type domain wall may be insensitive to the applied field around H_s. As will be discussed later, such weak field dependence of $\alpha(H)/\alpha(H_s)$ can be due to the complicated growth mechanism in the FR phase where another favorable A'/B'-type domain wall competes with the A'/C'-type one throughout the domain growth.

IV. MONTE CARLO RESULTS

A. Simulation procedure and H-T phase diagram

To understand the microscopic nature of the domain growth on the isosceles triangular lattice, MC simulations for the isosceles triangular lattice Ising model were performed. Instead of usual single-spin-flip method, a cluster heat bath algorithm[13] which treats a 1D magnetic chain as a cluster was adopted. We used the Ising Hamiltonian of Eq. (1), where $J_3/|J_2|\cos 2\theta_0=0.05$ was assumed. The periodic boundary condition was imposed along the directions on the isosceles triangular lattice, while along the chain the open boundary condition was imposed.

In Fig. 9, we show the magnetic phase diagram under applied fields parallel to the c axis, obtained by our MC simulations with size $12a\times24b\times25c$. The zero-field transition temperatures and critical fields were determined from the magnetic structure factor defined by

$$M(k)=\left|\sum_i \mathbf{S}_i \exp(2\pi i k y_i)\right|, \tag{5}$$

where k is a wave number in the b^* direction and y_i is a position of spin $\mathbf{S}_i$ in the b direction. The magnetic structure factor was calculated only for a wave number in the b^* direction because all the magnetic structures which appear under applied fields along the c axis are characterized by $q_{\rm propa}=(0\ q\ 0)$.[14] At each measuring temperature and magnetic field, $M(k)$ was averaged over 500 MC step (MCS) after discarding first 10^4 MCS. In our study, reduced temperature $T^*(=T/T_1^{\rm MC})$ and magnetic field H^* $(=H/H_c^{\text{AF-}FR})$ were introduced; $T_1^{\rm MC}/J_0S^2=0.9$ and $H_c^{\text{AF-}FR}$ is the AF-FR critical field. As expected from previous studies,[8] three magnetically ordered phases [AF $(q=\frac{1}{2})$, IC $(\frac{1}{3}<q<\frac{1}{2})$, and FR $(q=\frac{1}{3})$] were reproduced in our MC study.

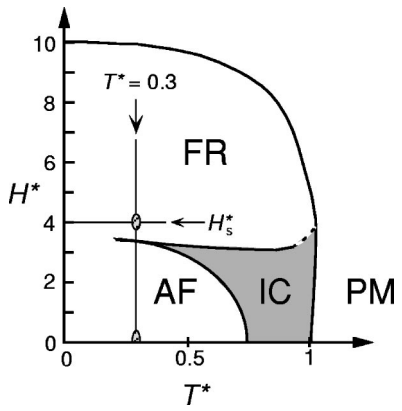

FIG. 9. Magnetic phase diagram obtained by MC simulations. The hatched areas show the magnetic-field region surveyed in present study.

The domain-growth kinetics after the quench from the PM disordered state was studied at $T^*=0.3$ for the system with size $96a\times96b\times25c$. The magnetic fields in the range $0\leqslant H^*\leqslant0.38$ for the AF state and in the range $3.75\leqslant H^*\leqslant4.25$ around H_s^* for the FR state were studied. Here, H_s^* $(=4.0)$ is the reduced magnetic field given by $2J_1S/(g\mu_B\cos\theta_0 H_c^{\text{AF-}FR})$, where the exchange field due to J_1 becomes of the same magnitude as the applied field and the A'/C'-type domain wall shown in Fig. 4(b) becomes free to shift along the b axis. By directly examining the spin configuration at every MCS, we counted the number of spin site that gives the phase shift in the sine-wave modulation, i.e., the number of domain walls. The spin-pair correlation function given by $G(r)=\langle\mathbf{S}_i\cdot\mathbf{S}_{i+r}\rangle-\langle\mathbf{S}_i\rangle^2$ was calculated and the magnetic correlation length along the a and b axes was defined as r, where $G(r)$ becomes a half the value at $r=0$. To obtain reliable sampling data, the data were averaged over ten different runs at each measuring field. Moreover, in order to avoid percolation effects, we stopped sampling the data at the MCS where the correlation length along the b axis becomes about one-fifth of the system size along the b axis.

Note that as is seen in the H^*-T^* phase diagram the critical fields between the FR and AF (or IC) phases determined on increasing field was found to shift toward a considerably high field; this field is below H_s, but far above $H^*=1$ expected from the mean-field theory. This may reflect the pinning effect that makes the spin state difficult to relax toward the equilibrium state.[7,15] Such effect can influence the growth exponent obtained by the simulations depending on the algorithm, although the feature of the domain growth is substantially unchanged.[7] Actually, in present Monte Carlo study the growth exponent both of the AF and FR states, obtained from the power-law fittings to the correlation length was in the range from 0.2 to 0.5 and was not uniquely determined. Nevertheless, we emphasize that the precise determi-

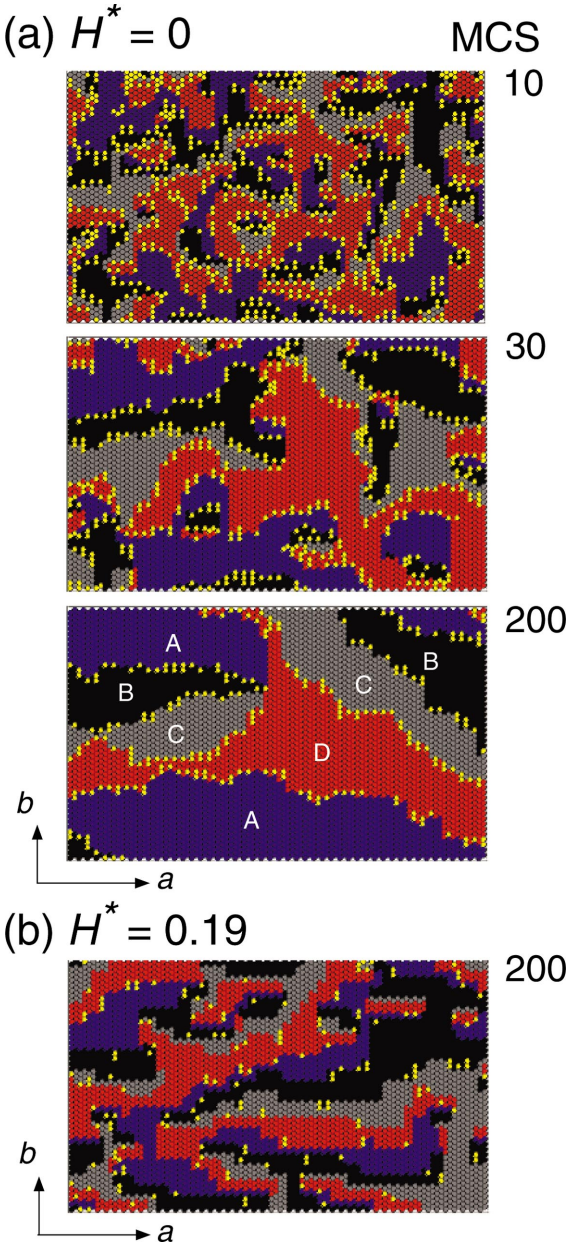

FIG. 10. (Color) The domain configurations in one isosceles triangular lattice plane of the system, taken at (a) $H^*=0$ and (b) $H^*=0.19$ in the AF phase. A $48a\times48b$ subsection of $96a\times96b$ lattice is shown. The blue, black, silver, and red areas show A,B,C,D domains, respectively. The yellow circles denote spins which flipped more than one time during the five MCS.

nation of the location of the phase boundary and growth exponent is far beyond our present purpose and that the pinning effect cannot substantially alter our conclusion.

B. Fourfold-degenerate AF phase

In Fig. 10(a), we show typical domain configurations in one isosceles triangular lattice plane of the system during the domain growth in zero field. These configurations were obtained by averaging spin configurations at this plane over five MCS; the spins which flipped more than one time during

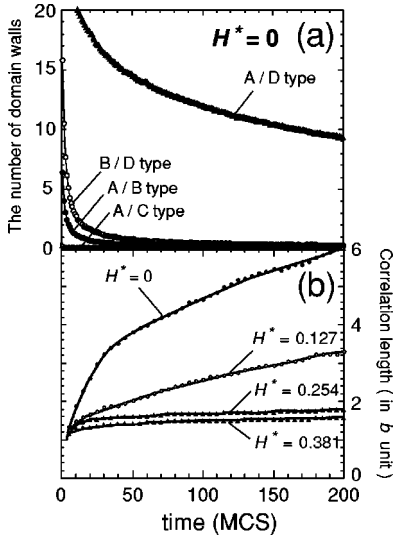

FIG. 11. (a) Time dependence of the number of domain walls in the b direction averaged over the a axis, taken at zero field in the AF phase. (b) Time dependence of the correlation length along the b axis under applied fields.

five MCS are denoted by yellow circles, while spins which did not reverse are used to identify each AF domain labeled as A, B, C, D denoted in Sec. II A. Figure 11(a) shows the time dependence of the number of domain walls in the b direction at zero field. Just after the quench unfavorable B/D-, A/B-, and A/C-type domain walls diminish rapidly and the most favorable A/D-type domain wall dominates throughout the domain growth and decreases with time. Correspondingly, the number of flipped magnetic chains, which is considered to contribute to the susceptibility, decreases with time as shown in Fig. 10(a).

As the magnetic field is applied, magnetic chains are less flipped and the large number of domain walls remain in the b direction even at 200 MCS as seen in the domain configuration at $H^*=0.19$ in Fig. 10(b). This behavior is reflected in the time dependence of the correlation length along the b axis shown in Fig. 11(b); the correlation length at 200 MCS systematically decreases with increasing magnetic field. This indicates that the magnetic field has a slowing-down effect on the domain growth in the AF phase.

It should be emphasized that the time dependence of peak position in the AF phase after RH obtained from our neutron-scattering results[9] can be explained by the formation of the A/D-type domain wall in the b direction. As shown in Fig. 12, in the $(3\ k\ 0)$ reciprocal-lattice scan it was found that just after RH the magnetic peak in the b^* direction appears at k slightly smaller than 0.5 of the AF peak position and approaches 0.5 with time. Under the magnetic field, the deviation of the peak position from 0.5 becomes pronounced compared with the zero-field case. As our MC results showed, in $CoNb_2O_6$ the A/D-type domain wall is expected to be dominant and the thermodynamically equivalent AF domains will arrange along the b direction like $A/D/C/B/A/D$ as shown in Fig. 2(f). Just after RH, the correlation length along the b axis is not so large, therefore, this arrangement causes the

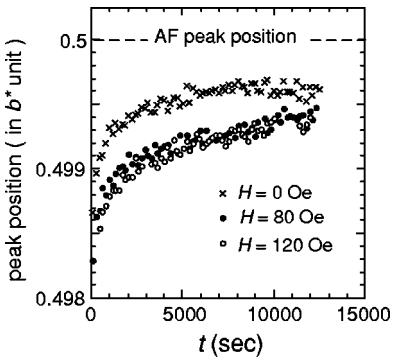

FIG. 12. Time dependence of the peak position in the (3 k 0) reciprocal-lattice scan in the AF phase after RH, obtained from our neutron-scattering studies (Ref. 9).

magnetic peak with q close to 0.5 in the neutron-scattering measurements. Particularly, in the (3 k 0) reciprocal-lattice scan, the peak position should be less than 0.5. On the other hand, if the different types of domain wall are arranged in the b direction, the magnetic peak position in the (3 k 0) reciprocal-lattice scan should be slightly greater than 0.5 for the A/B type or exactly at 0.5 for the A/C type and B/D type. Therefore, the observed peak position shown in Fig. 12 strongly supports the formation of the A/D-type domain wall in this system. As the domain growth proceeds, AF network within each domain develops and the distance between adjacent domain walls in the b direction increases. This makes the peak position more closer to 0.5, being responsible for the time dependence of the peak position toward 0.5 shown in Fig. 12.

C. Threefold degenerate FR phase

Figures 13(a)–13(c) show the time dependence of the number of domain walls in the b direction at $H^*=3.87$, 4.0, and 4.13, respectively, around the specific field of H_s^* (=4.0). In Fig. 14 the domain configuration at 200 MCS at $H^*=H_s^*$ is shown. Just after the quench, the energetically favorable A'/C'-type domain wall being mobile at H_s^* is dominant and its amount decreases with time. However, at all measuring field the A'/B'-type domain wall persists even at the later stage. While magnetic chains close to the A'/C'-type domain wall flip frequently, those close to the A'/B'-type domain wall less flip as shown in Fig. 14. This behavior is in contrast with the AF case where only one type of domain wall controls the domain growth in the system.

With slightly changing the magnetic field from H_s^* the time evolution of the correlation length along the b axis is suppressed as shown in Fig. 13(d). The behavior around H_s^* is strongly asymmetric with respect to H_s^*, which is reflected in the temporal behavior of the number of the domain wall shown in Figs. 13(a)–13(c).

Now we discuss the growth mechanism around H_s^*. Just after the quench, thermodynamically equivalent three FR domains (A',B',C') nucleate and three types of domain walls shown in Figs. 4(a)–4(c) are formed in the b direction. Particularly at $H^*=H_s^*$ the C'/A'-type domain wall which includes two unstable up magnetic chains is energetically unstable, therefore either of two magnetic chains will reverse downward just after the C'/A'-type domain wall is formed. As a consequence, the C'/A'-type domain wall transforms into the A'/B'-type domain wall and the two types of domain wall (A'/B' and A'/C' types) compete throughout the domain growth as shown in Fig. 13(b). However, in contrast to the A'/C'-type domain wall, the A'/B'-type one is immobile along the b axis because all the magnetic chains close to the domain wall have large activation energy to reverse. This makes the A'/B'-type domain wall stable during the domain growth as shown in Fig. 13(b).

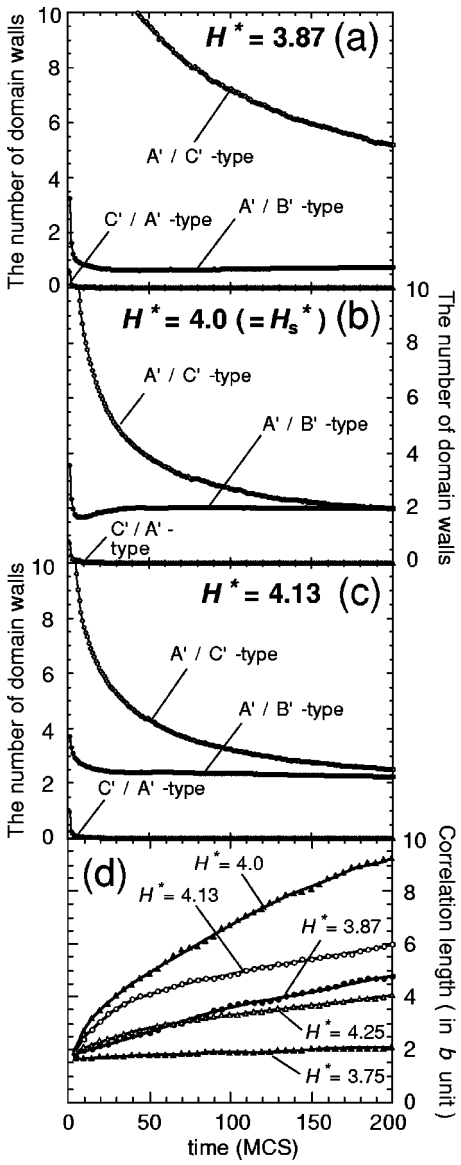

FIG. 13. Time dependence of the number of domain walls in the b direction averaged over the a axis, taken at (a) $H^*=3.87$, (b) $H^*=4.0$, and (c) $H^*=4.13$ in the FR phase. (d) Time dependence of the correlation length along the b axis under applied fields around H_s^*.

With slightly changing the magnetic field from H_s^*, the situation changes dramatically depending on whether applied

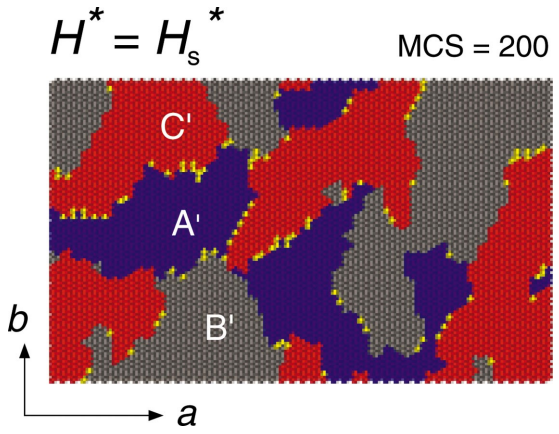

FIG. 14. (Color) The domain configuration in one isosceles triangular lattice plane of the system, taken at $t=200$ MCS during the domain growth at $H^*=H_s^*$. A $48a\times48b$ subsection of $96a\times96b$ lattice is shown. The blue, silver, and red areas show A', B', C' domains, respectively. The yellow circles denote spins which flipped more than one time during the five MCS.

field is larger than H_s^* or not. This originates from the different decay process of the unstable C'/A'-type domain wall around H_s^*. When $H^*<H_s^*$, also the magnetic chains which are free at H_s^* [double circles in Fig. 4(c)] become energetically unstable. Therefore, it is possible that certain number of the C'/A'-type domain walls decay to the A'/C'-type one by the reversal of such unstable magnetic chains. On the other hand, when $H^*>H_s^*$, the situation is similar to that at $H^*=H_s^*$ and the transition toward the A'/C'-type domain wall is not likely to occur. The decay process of the C'/A'-type domain wall depending on the magnetic field leads to different population of the A'/C'-type domain wall at $H^*=3.87$ [Fig. 13(a)] and $H^*=4.13$ [Fig. 13(c)] and is responsible for the asymmetric time evolution of the correlation length around H_s^* shown in Fig. 13(d).

In present MC study, we have shown that the growth mechanism around the specific field of H_s is controlled by the two types of domain walls. Experimentally, however, it is difficult to extract the time-dependent behavior of the A'/B'- and A'/C'-type domain walls separately from the ac susceptibility data, because ac susceptibility is sensitive only to the domain wall which includes free magnetic chains. Only the high-Q neutron scattering or magnetic x-ray scattering may distinguish these two types of domain walls, because in the reciprocal-lattice space, the domain-wall configuration due to the A'/B' and A'/C' types gives different magnetic peak position in the b^* direction, around the FR position at $k=\frac{1}{3}$ and $\frac{2}{3}$. Detailed study of the domain growth in the FR phase by means of the scattering technique will appear elsewhere.

V. CONCLUSION

The domain growth of highly degenerate ground states has been investigated in the isosceles triangular Ising antiferromagnet $CoNb_2O_6$ by ac susceptibility measurements and Monte Carlo simulations. Ac susceptibility after the field quench decreases with time and shows the power-law time dependence with an *universal* growth exponent $n=0.21\pm0.01$ both in the fourfold-degenerate AF and field-induced threefold-degenerate FR phases.

In the AF phase, the prefactor in the power-growth law which is a measure of the relaxation speed was found to increase rapidly with increasing applied field. This result indicates that the application of the magnetic field perpendicular to the isosceles triangular lattice plane strongly suppresses the domain growth in the AF phase. Monte Carlo simulations showed that the exchange field at the magnetic chain near the favorable domain wall is exactly canceled out under the isosceles triangular geometry and the domain-wall motion due to the reversal of such *free* magnetic chain dominates the domain growth. With slightly applying the magnetic field, the thermal fluctuation of free magnetic chain is suppressed owing to the presence of the finite activation energy against the applied field and the domain growth becomes slower, being responsible for the field dependence of the prefactor in the power-growth law. Moreover, we showed that at the late stage thermodynamically equivalent four AF domains arrange in the modulated direction (b direction) with a phase shift of $\pi/2$ at the domain wall and this observed domain configuration explains well the temporal shift of the magnetic peak position toward the AF one, observed in our neutron-scattering measurements.

On the other hand, around the specific field of H_s ($=1214$ Oe) in the FR phase, the prefactor in the power-growth law is less field independent, although the reversal of free magnetic chains and its suppression under the applied field far from H_s are expected as is in the AF case. Monte Carlo simulations showed that in contrast to the AF phase where a single type of domain wall dominates, two types of favorable domain walls compete throughout the domain growth around H_s. This results in asymmetric field dependence of the domain growth around H_s.

The obtained growth exponent of $CoNb_2O_6$ is the universal value of 0.21 and is anomalously low compared with $\frac{1}{2}$ of a conventional Ising magnet. This universal exponent implies the existence of the underlying universal growth mechanism governing the growth law in this system. As our Monte Carlo simulation showed, the domain growth in $CoNb_2O_6$ is dominated by the reversal of *free* magnetic chains on the frustrated isosceles triangular lattice. Therefore, its reversal will occur stochastically and the domain growth will be controlled by the stochastic motion of the domain wall, although that of a conventional system is driven by reducing the curvature of the domain wall.[1] Such growth mechanism might make the domain growth extremely slower and might cause the observed low exponent in $CoNb_2O_6$. In fact, a low growth exponent of 0.25 was reported in an antiferroelectric $K_2Ba(NO_2)_4$ where the rearrangement of free 2D planes of electric dipole moments takes place on a frustrated triangular lattice.[16] Future theoretical works are required to give deeper understanding of the anomalous growth exponent of $CoNb_2O_6$.

ACKNOWLEDGMENTS

We would like to thank Professor Kay Kohn of Waseda University for supplying single crystals used in present study. We thank T. Kasahara, S. Kawasaki, S. Fujisaka, and S. Taniguchi for their assistance of Monte Carlo simulations. This work was partly supported by the Science Research Promotion Fund of the Promotion and Mutual Aid Corporation for Private Schools of Japan.

*Present address: Institute of Multidisciplinary Research for Advanced Materials, Tohoku University, Sendai 980-8577, Japan. Electronic address: koba@tagen.tohoku.ac.jp

[1] J.D. Gunton, M. San Miguel, and P.S. Sahni, in *Phase Transitions and Critical Phenomena*, edited by C. Domb and J.L. Lebowitz (Academic Press, London, 1983), Vol. 8, p. 267.

[2] *Dynamics of Ordering Processes in Condensed Matter*, edited by S. Komura and H. Furukawa (Plenum, New York, 1988).

[3] I.M. Lifshitz, Zh. Éksp. Teor. Fiz. **42**, 1354 (1962) [Sov. Phys. JETP **15**, 939 (1962)].

[4] T. Ala-Nissila and J.D. Gunton, Phys. Rev. B **38**, 11 418 (1988).

[5] K. Kaski, T. Ala-Nissila, and J.D. Gunton, Phys. Rev. B **31**, 310 (1985); T. Ala-Nissila, J.D. Gunton, and K. Kaski, *ibid.* **37**, 179 (1988).

[6] G.N. Hassold and D.J. Srolovitz, Phys. Rev. B **37**, 3467 (1988).

[7] M. Cheon and I. Chang, Phys. Rev. Lett. **86**, 4576 (2001).

[8] S. Kobayashi, S. Mitsuda, M. Ishikawa, K. Miyatani, and K. Kohn, Phys. Rev. B **60**, 3331 (1999).

[9] S. Kobayashi, S. Mitsuda, T. Jogetsu, J. Miyamoto, H. Katagiri, and K. Kohn, Phys. Rev. B **60**, R9908 (1999).

[10] Incorrectly, the prefactor for $\xi_b(t)$ shown in Fig. 4(b) in Ref. 9 was 4π times larger value.

[11] Y. Kuramitsu, K. Amaya, and T. Haseda, J. Phys. Soc. Jpn. **33**, 83 (1972); M. Motokawa, *ibid.* **35**, 1315 (1973).

[12] A. van der Bilt and A.J. van Duyneveldt, Physica B **95**, 305 (1978).

[13] O. Koseki and F. Matsubara, J. Phys. Soc. Jpn. **66**, 322 (1997).

[14] S. Kobayashi, S. Mitsuda, and K. Prokes, Phys. Rev. B **63**, 024415 (2001).

[15] A. Sato and F. Matsubara, Phys. Rev. B **60**, 10 316 (1999).

[16] Y. Noda, in *Phase Transitions and Critical Phenomena* (Ref. 2), p. 333.